Multianalytical characterization of Late Roman glasses including nanosecond and femtosecond laser induced breakdown spectroscopy

M. Oujja[1*], M. Sanz[1], F. Agua[2], J.F. Conde[2], M. García-Heras[2], A. Dávila[3], P. Oñate[4], J. Sanguino[4], J. R. Vázquez de Aldana[5], P. Moreno[5], M.A. Villegas[2], M. Castillejo[1]

[1] Instituto de Química Física Rocasolano, CSIC, Serrano, 119, 28006 Madrid, Spain

[2] Instituto de Historia, CCHS-CSIC, Albasanz, 26-28, 28037 Madrid, Spain

[3] Consejería de Educación, Cultura y Deportes, Juan Bautista Topete 1-3, Guadalajara, Spain

[4] GABARK Consultores Patrimonio Histórico, S.L. Avda. de la Peseta, 78, 28054 Madrid, Spain

[5] Grupo de Investigación en Microprocesado de Materiales con Láser, Universidad de Salamanca, Plaza de la Merced s/n, E-37008, Salamanca, Spain

[*] E-mail: m.oujja@iqfr.csic.es

Abstract

In the present study, a historical set of Late Roman glasses coming from a recently unearthed graveyard located in the small city of Cubas de la Sagra, within the Madrid region (Spain) was compositionally analysed using different techniques such as ultraviolet-visible (UV-Vis) and laser induced fluorescence (LIF) spectroscopies, X-ray fluorescence (XRF) and laser induced breakdown spectroscopy (LIBS). LIBS results, recorded upon nanosecond (ns) and femtosecond (fs) laser irradiation, served for identification of major glass components (to classify them into main historical glass groups) and of minor components (e.g. chromophores, decolouring agents and degradation products). Quantitative information regarding these components was obtained on the basis of calibration curves obtained using glass certified standards and local standards. We have demonstrated that LIBS serves for the non-invasive/micro-destructive, quantitative chemical characterization of most of the analysed historical glasses. Furthermore, this work establishes a comparison between LIBS analysis of glasses in the ns and fs regimes on one hand, and on the other hand with the results obtained

1

using XRF. The procedures and protocols here proposed can be applied for *in-situ* study of

historical glass collections, regardless of their size, provenance and chronology.

Introduction

Laser induced breakdown spectroscopy (LIBS) is a useful method for determining the elemental composition of a large number of materials in different environmental conditions such as air at atmospheric pressure, vacuum or water.[1-10] As no material pre-treatment is needed and due to the swiftness of analysis, this technique offers an attractive solution for a wide range of applications.[8-11] The analytical performance of LIBS depends strongly on the choice of experimental conditions that influence the laser-produced plasma characteristics.[12,13] The main parameters affecting the performance of LIBS are the laser intensity, excitation wavelength, laser pulse duration, physical and chemical properties of the target material and its surface conditions, and the surrounding atmosphere.[2] Although many studies have been undertaken to investigate the influence of these factors, there is relatively less knowledge available about the influence of laser pulse duration on LIBS analysis.[14-16] With the introduction of ultra-short laser pulses in the picosecond (ps) and femtosecond (fs) ranges, a large interest in investigating the advantages offered by these laser sources for spectrometric applications, such as LIBS, has been developed both in single or double pulse approaches.[14,17-20] The physical mechanisms involved in ultrashort fs laser ablation differ from those taking place with nanosecond (ns) pulses. Because of their very short duration, fs pulses do not interact with the resulting plasma; thus the absorbed laser energy is fully deposited into the material at the solid density, with little thermal diffusion while the pulse is on. The shortening of laser pulse duration decreases the size of the heat-affected-zone and leds to more controllable material modification and removal. The reduced thermal effects also help to achieve stoichiometric ablation which improves the analytical performance of the technique. On the other hand, for longer ns pulses, increased heat conduction takes place inside the target during ablation and significant laser energy is absorbed by the expanding

3

plasma, which increases the efficiency of conversion from laser energy to plasma energy and thus to radiation.

Common laboratory-based techniques used for characterizing historical glasses, such as X-ray fluorescence spectrometry (XRF) and scanning electron microscopy/energy-dispersive X-ray spectroscopy (SEM/EDX), are usually destructive, as sampling is necessary and the removed material has to be ground for analysis. Although portable XRF systems are becoming more available, the above mentioned techniques cannot be applied for non-destructible samples of considerable or relatively big size, from museum collections, or for glass items that must be reintegrated into a work of art, as for instance, stained glass windows. Although LIBS has been used in several archaeometrical studies of different cultural heritage materials,[21-26] those devoted to historical glasses are scarce. These studies have focused on finding the optimal LIBS parameters for the analysis of model soda lime silicate[27] and historical lead silicate glasses,[28] on the characterization of chromophores and opacifiers of ancient glasses, and on degradation pathologies.[29-31] LIBS has proved to be effective for studying glasses from a wide variety of perspectives.[27-33] However, the potential of LIBS as a micro-destructive technique for quantitative bulk chemical composition analysis of ancient glasses remains almost unexplored.

For quantitative compositional material analysis by LIBS, two approaches are available. The widely used calibration-based method relies on certified reference materials which are measured by LIBS.[28,33] Calibration curves are derived for specific elements that are used to determine their content in the substrate under study. To achieve good level of detection it is necessary to use matrix-matched reference materials and to apply similar experimental conditions for measuring the samples and the references. The second technique is based on a calibration-free procedure, where the laser-induced plasma and the optical plasma emission

are modeled and directly yield the composition of the sample material from the LIBS spectra.[32,34]

In the present work we present a comparative quantitative analysis by LIBS of an outstanding set of Late Roman glasses using both ns and fs laser pulses. Calibration curves were obtained based on LIBS measurements on standard and certified glasses. The obtained results were compared and integrated with those provided by XRF, Ultraviolet-Visible spectroscopy (UV-Vis) and Laser Induced Fluorescence (LIF).

Experimental

Description of samples

The study focuses on a set of glass fragments of the Late Roman period from a recently unearthed graveyard located in the small city of Cubas de la Sagra (Madrid region, Spain). Fig. 1 shows pictures of the selected glass fragments. The graveyard, which is associated to an important craftsmen settlement site, is constituted by two zones only separated by 200 m. The first area (Area 1), of approximately 80 m^2, has been completely excavated and has provided 10 graves, whereas the second area (Area 2), of nearly 10.500 m^2 and still partially excavated, has provided 142 graves up to now, even though at least 119 other have been located. The graves identified in both areas have been dated between late fourth and mid fifth century AD and mainly correspond to individual burials oriented NW-SE. Only 24 graves have provided goods consisting of ceramic vessels and glass recipients while glass fragments have been found in only 18 of these 24 graves. Such fragments belonged presumably to bowls and beakers, mainly in the 96 Isings form.[35] Colourless and olive green are the predominant colours of the excavated glass items. Nine glass samples (two from Area 1 and seven from Area 2) have been selected for the investigation herein. Table 1 lists the main characteristics of these samples.

Analytical techniques

The glass samples were compositionally analysed using a set of analytical techniques including XRF, UV-Vis, LIF and LIBS.

Chemical analyses by XRF were carried out with a PANalytical Axios wavelength dispersed X-ray spectrometer equipped with a rhodium tube of 4 kW and 60 kV. Analytical determinations were undertaken through the standard-less analytical software IQ+ (PANalytical) from synthetic oxides and natural minerals. XRF analyses were carried out on powder samples prepared by grinding body glass fragments, with their most external surfaces removed, by polishing in an agate mortar.

UV-Vis spectra of the samples were acquired with an Ocean Optics HR 4000 CG system. Spectra were recorded in the 250-1100 nm range on glass sections of approximately 1 mm in thickness, obtained by polishing both sides for optical quality.

LIF measurements were carried out using laser excitation at 266 nm (4th harmonic of a Q-switched Nd:YAG laser, 6 ns pulses, 10 Hz repetition rate) and a 0.30 m spectrograph with a 300 grooves/mm grating (TMc300 Bentham) coupled to an intensified charged coupled detector (2151 Andor Technologies). The temporal gate was operated at zero time delay with respect to the arrival of the pulse to the surface of the sample and with a width of 3 μs. The sample was illuminated by the laser at an incidence angle of 45° with pulses of around 0.1 mJ. For the results presented here, a 420 nm cutoff filter was set in front of the spectrograph to avoid the second order emissions of lower wavelengths. Each spectrum resulted from the accumulation of 20 measurements in five different points of each sample zone.

LIBS analysis was performed using two different systems based on ns and fs lasers. The first system consists of both the laser source and the spectrograph-ICCD detection systems described above for acquisition of LIF spectra. The laser beam was also directed to the surface of the glass samples by the use of mirrors at an incidence angle of 45°. We used

irradiation fluences of 6.6 J cm^{-2} by focusing with a 10 cm focal length lens, to a spot diameter size of 240 μm, pulses of 3 mJ. This fluence ensures a good signal/noise ratio and good reproducibility of LIB spectra. The shot to shot laser energy fluctuation was less than 10 % and LIB spectra were recorded at 70 nm intervals with a 300 grooves/mm grating in the 250–600 nm wavelength range at a 0.025 nm resolution. A cut-off filter at 320 nm was placed in front of the entrance window of the spectrograph to reduce the scattered laser light from the surface of the sample and to avoid the second-order diffraction. The gate delay and width were adjusted to both minimize the early continuous bremsstrahlung emission and maximize the light emitted by ionized species present at the initial stages of the ablation plasma and which usually contains useful analytical information. We noticed that contribution of bremsstrahlung was negligible even at zero time delay (see section on LIBS below) and selected values of 0 and 1 μs for gate delay and width respectively. Spectra resulted from summing up the emissions from ten successive laser pulses, which helped to improve even more the signal/noise ratio.

The second LIBS system is based on a commercial Ti:Sapphire oscillator (Tsunami, Spectra Physics) and a regenerative amplifier system (Spitfire, Spectra Physics) based on the chirped pulse amplification technique. This laser produces linearly polarized 120 fs pulses at 800 nm with a repetition rate of 1 kHz. The pulse energy can reach a maximum of 1 mJ and it is finely controlled by a half-wave plate and a linear polarizer. For ablation, the laser beam spot was concentrated on the surface of the sample to a diameter of 32 μm with a 10 cm focal length lens. Reproducible spectra with good signal/noise ratio were obtained using pulse energies of 200 μJ yielding fluences of 24 Jcm^{-2}. The LIB spectra were recorded using a spectrograph (Shamrock SRS 303i) coupled to time gated ICCD camera (iSTAR DH734i-18F-03 Andor Technologies) with a 0.025 nm resolution. In this case the spectra were obtained by accumulation of the signal produced by ablation with fifty successive laser pulses at the

maximum repetition rate of the laser of 1 KHz. The plasma generated during the interaction of fs laser pulses with the sample leaves the ablation region at very high speeds (in the range of thousands of m/s). The interaction of a given incoming pulse with ablated species produced by the previous one (arriving at the target 1 ms earlier) is negligible and the LIBS signal recorded by accumulation of successive pulses is the simple addition of individual single pulse emissions. As in the ns-based LIBS system previously described, we optimized the spectral acquisition for the best reproducibility and signal/noise ratio using a gate delay and width of 0 and 1 μs, respectively.

The comparison between ns and fs LIBS results was based on the best performance for each approach, by considering in each case fluence and temporal gate parameters that allow the best reproducibility and signal/noise ratio. No attempt was made to use comparable ns and fs pulse energies because of the difficulty of inducing reproducible ablation sparks at very low energies by using ns excitation.

Results and discussion

X-ray Fluorescence

The historical Late Roman glasses were quantitatively analyzed by XRF. Table 2 shows the chemical composition determined by this technique. In all the analyses SiO_2 and Na_2O are the major components, with contents in wt.% ranging between 63-68 and 16-19, respectively. Historically, a high SiO_2 and Na_2O content ensured the improvement of the glass chemical resistance. Small amounts of other oxides, eg. Fe_2O_3, MnO and CuO are also found. These oxides were added to the raw materials with the intention of colouring the glass. Other minor components found (Al_2O_3, MgO, BaO, PbO, etc.) can be attributed to impurities of the raw materials employed in the manufacturing process.

Besides the historical glasses, standard and homemade model glasses were analyzed and used as calibration patterns for LIBS quantitative determinations. The obtained results are

8

displayed in Table 3. The standard glasses are soda-lime-silica glass (Gl-1, standard glass Nº 7), lead oxide-potassium oxide-silica glass (Gl-2, standard glass Nº 8) and amber soda-lime-silica glass (Gl-3, SGT 10) provided by the Society of Glass Technology, UK. The homemade model glasses (Gl-4 to Gl-7) were prepared on the occasion of a previous study[28], and were chosen due to the similar chemical composition as the historical ones subject of the present investigation.

UV-Vis spectroscopy

The colour characterization of glasses, i.e. the detection of their chromophores, was done by UV-Vis spectroscopy. Among the set of samples, representative colourless, olive green, yellowish colourless, bluish colourless and blue colorations were selected. All the samples studied show one of these colours (Table 1, Fig. 1). Small pieces of the samples to be analyzed were cut and polished to optical quality by both sides and, when necessary, they were transformed into plano-parallel slabs, with thickness equal or less than the original thickness of the glass samples as received.

Fig. 2 shows the UV-Vis spectra of some of the samples studied (CS-1, CS-4, CS-8, CS-9 and CS-10). The spectrum of the olive green glass CS-1 (Fig. 2a) presents absorption bands due to the pair Fe^{2+}/Fe^{3+}, at 420 and 440 nm, assigned to Fe^{3+} (yellow colour) and at around 1050-1100 nm assigned to Fe^{2+} (blue colour). The simultaneous presence of both oxidation states of iron ions causes the chromatic addition of their respective absorption bands, which explains its green colour. Therefore the olive hue of the CS-1 green glass (Fig. 1) comes from the relative intensity of the bands of both oxidation states of iron ions. This result is confirmed by the chemical composition derived from the XRF analysis. The total iron oxide concentration of this sample is 2.31 wt. %, as reported in Table 2. The 2.48 wt. % content of manganese oxide for this sample is too low to produce an effective discoloration effect. This aspect will be detailed below.

The spectrum of the colourless glass CS-4 is shown in Fig. 2b. In this case the absorption bands of the two oxidation states of the pair Fe^{2+}/Fe^{3+} were also observed, although with lower intensity as compared to Fig. 2a. In fact, the total iron oxide percentage of this glass sample determined by XRF (Table 2) is as low as 0.50 wt. %. Such amount of iron ions is not able to produce the residual greenish hue observed in sample CS-1. The absence of colour of CS-4 can be also explained by the presence of another chromophore, the Mn^{3+}, whose absorption band at around 500 nm (pink colour) compensates the greenish coloration produced by iron ions. In fact, XRF results displayed in Table 2 confirm this statement, since the manganese oxide content detected by XRF in glass CS-4 is higher than 1 wt. %. The use of manganese salts as a decolouring agent of glasses was well known by Roman glass-makers, who inherited this tradition from Assyrian glass artisans.[36]

The spectrum of Fig. 2c, which corresponds to the yellowish glass CS-8, is very similar to that shown in Fig. 2a. In this case, although both bands due to iron ions are present, the colour eventually looks yellowish instead of green, because the relative intensity of the absorption bands of Fe^{3+} (yellow) is higher than the corresponding to the band of Fe^{2+} (blue). The opposite case appears in Fig. 2d for the bluish sample CS-9, in which the intensity of bands of Fe^{2+} is higher than that of Fe^{3+}. The presence of iron ions as chromophores in glasses CS-8 and CS-9 was confirmed by XRF analyses (Table 2). In sample CS-8 the content of iron oxide detected was 1.51 wt. %, while it was 0.64 wt. % in sample CS-9. It is important to note that sample CS-8 also contains a noticeable amount of manganese oxide (2.53 wt. %) that prevents, by means of the chromatic compensation mentioned above, a greenish appearance due to iron ions.

In Fig. 2e the spectrum of the blue glass CS-10 is shown. Besides the absorption bands assigned to Fe^{2+}/Fe^{3+}, a band due to Cu^{2+} appears at about 800 nm. The blue colour produced by Cu^{2+} masks the light yellow colour due to Fe^{3+}. As it can be seen in Table 2, copper oxide

and iron oxide contents of glass CS-10 are about 1 wt. %. This sample also contains 1.31 wt. % of manganese oxide, but in this case the manganese ions are unable to chromatically compensate the blue colour provided by Cu^{2+}-ions.

As regards the production technology involved in producing the different colours observed in the set of glasses studied, the chromophores detected by UV-Vis spectroscopy indicate that yellowish and bluish hues could be the result of iron oxide impurities of the sand used for glass-making. The intense olive green colour comes from to one of these origins: a) intentionally added iron oxide for colouring; b) the use of sands containing high quantities of iron oxide impurities; c) the use of recycled glass, in which the iron impurities are concentrated and the mixture of different original colours is common. Among these three options, the third arises as the most probable, since, as it is well documented,[37-39] in the 4-5th centuries AD the practice of recycling glass was widely extended throughout the Roman Empire.

Laser Induced Fluorescence

LIF spectra were collected on the bare surface of the samples upon laser excitation at 266 nm for each of the nine glasses selected for this study. Fig. 3 displays representative spectra.

Fig. 3a shows the spectrum of the olive green CS-1 glass, which consists of three broad bands centered at 350, 440 and 655 nm. The emission observed at 350 nm was assigned to Fe^{2+}/Fe^{3+} chromophores.[40,41] The bands at 440 and 655 nm correspond to the contribution of different glass fluorophores and to the Mn^{3+} chromophore,[42] respectively. As shown before, the presence of these bands in the UV-Vis spectra (Fig. 2) supports such assignment. The colorless CS-4 glass (Fig. 3b) displays the same LIF spectrum as that of CS-1 at reduced intensity. This decrease in intensity explains the absence of colour of CS-4 glass. The relative intensity of the bands observed in the LIF spectra of the remaining analyzed glasses, CS-5, CS-7, CS-8 (in Fig. 3c), CS-9 (in Fig. 3d), CS-11 and CS-12, is related to the content of iron

and manganese oxides which defines their coloration. For CS-10 glass (Fig. 3e), in addition to the bands observed for the previous glasses, an additional over-imposed band, attributed to the Cu^{2+} chromophore is observed at 475 nm.[43] The presence of the Cu^{2+} is responsible for the blue colour of CS-10 glass. This result is in agreement with those obtained using UV-Vis spectroscopy reported above.

Laser Induced Breakdown Spectroscopy

LIB spectra were recorded in the glass samples by ns and fs laser excitation. The spectra revealed their elemental composition according to the emission lines of main and minor components, including the chromophore compounds responsible of their colour. As an example, Fig. 4 shows the LIB spectra of sample CS-10 recorded using ns and fs pulses. The emission lines were assigned based on data from.[45] In the different samples examined (CS-1 to CS-12) we detected lines of iron, manganese and cooper which are linked to the present chromophores, as ascertained by UV-Vis and LIF analysis. Lines of barium, chromium, chlorine, titanium and lead are related to the presence of glass impurities. Emission lines of the main glass components, such as silicon, sodium, calcium, magnesium, aluminum and potassium, were observed for all analyzed samples. We observed that the elemental composition of the historical glasses determined by ns and fs LIBS did not differ significantly, as we detected the same set of elements for each sample in both temporal regimes.

We investigated the influence of laser pulse duration on the plasma characteristics, in particular the number of lines and their relative intensities. As observed in Fig. 4, the line intensity of the major elements in the case of ns pulses (Fig. 4a) is higher than those observed by excitation with fs pulses (Fig. 4b). It is also noticed that, by using the same delay and gate width for signal acquisition, the LIB spectra acquired with ns pulses are richer in line emissions than those corresponding to fs pulses. These differences have their origin in the

varying ablation and plasma expansion dynamics taking place with ns and fs pulses. During the interaction of ns laser with the solid, the pulse energy is transferred to the electrons of the lattice, resulting in melting and vaporization of the target. This is followed by the expansion of a vapour plume, which induces a shock wave assisting the ionization of the surrounding gas. Furthermore, the laser pulse interacts with the plasma, leading to efficient reheating by inverse bremsstrahlung absorption.[44] However, for fs pulses the time scale is shorter than the electron cooling time and the lattice is instantaneously heated, resulting in plasma formation of the vapour and expansion phase.

Table 5 presents a summary of the elemental composition of each historical glass sample as determined by LIBS. The comparison with data derived from XRF (Table 2) reveals that LIBS is able to detect the presence of most of the elements of the compounds identified by XRF, except the elements P, S, Sb, B, As and Zr. This is due to the difficulty to detect these elements in the considered spectral range (250-600 nm) or to their very low content. However, it was observed that the element chromium was easier to detect by LIBS (especially in the ns mode) than by XRF.

In order to perform quantitative LIBS analysis we obtained calibration curves for the elements appearing in the spectra of the historical glass samples (listed in Table 4). To that purpose we measured LIB spectra, with both ns and fs excitation, of the standard and homemade model glasses listed in Table 3. The line intensities corresponding to a given element in the glass samples were normalized to the Si I emission at 288.16 nm, which was used as an internal standard. This procedure is a common approach in LIBS analysis[27] and serves to minimize the fluctuations that can arise from matrix effects and laser instability. For quantification of Si itself, the intensity of line at 288.16 nm, was normalized to the intensity of another line of the same element at 390.55 nm. The corresponding relative intensities were represented as a function of the wt. % content of the compound containing that element as determined by XRF

(Table 3). The element Sr, which was detected by LIBS in the Late Roman glasses, could not be quantified due to its absence in the standard and model glasses.

Fig. 5 presents a selection of the calibration curves obtained, for both ns and fs laser irradiation, specifically those for Na I (330.23 nm), Mg I (285.21 nm), Al I (309.27 nm) and Fe I (438.35 nm). The standard deviation, shown with error bars, of the data points for the ns case was significantly lower than that obtained with fs pulses, owing essentially to the more stable energy output of the ns laser and to the effect on line emission intensity of the glass surface roughness for fs pulses. The calibration curves for ns LIBS analysis show a fairly good linearity, with correlation coefficients near unity (0.92-0.98). However, for fs irradiation the calibration curves depart from linearity with correlation coefficients ranging from 0.57 to 0.93.

Table 5 also shows the results of the quantitative analysis obtained from the described calibration procedure for ns and fs pulses. For the main elements of glasses, silicon and sodium, the elemental composition derived from the ns and fs analyses differs in less than 10 %. For the rest of elements detected the differences vary, although in some cases can overcome 100 %. As regards the quantitative comparison with XRF results the differences range from 3 to 20 % for main components silicon and sodium and reach considerably higher values for minor components. It is observed that the agreement, in quantitative terms, between LIBS and XRF results, is better achieved in the ns mode owing to the better linearity of calibration curves obtained in this case.

Conclusions

The technique of laser induced breakdown spectroscopy has been used to analyze the chemical composition of non-destructible historical Late Roman glasses in an integrated analytical approach, which includes, UV-Vis and laser induced fluorescence spectroscopies and X-ray fluorescence (XRF). LIBS allowed the detection of major, minor and trace

elements in glasses and the quantitative determination of different compounds for a wide range of concentrations.

Nanosecond and femtosecond laser irradiation yielded almost similar qualitative results, although the LIB spectra acquired in the nanosecond mode contained more line emissions of higher intensities than in the femtosecond mode. Additionally, ns LIBS featured higher sensitivity for minor components such as Cr and Ba. The differences between LIBS results obtained in the two temporal regimes are attributed to characteristics of plasma expansion dynamics, to varying pulse to pulse fluctuations of ablation pulse energies and to differences in analysis protocols.

For the quantitative data regarding glass chemical composition, nanosecond and femtosecond LIBS results were validated by comparison with those obtained by XRF using a calibration-based method relying on standard and homemade model glasses. Calibration curves for nanosecond LIBS analysis showed better linearity compared to those obtained with femtosecond pulses. For the Late Roman glasses studied this fact led to a more satisfactory agreement, in quantitative terms, between nanosecond LIBS and XRF results.

Consequently it can be concluded that LIBS constitutes a powerful technique to determine glass chromophores and to look for chemical differences or similarities in the body of non-destructible samples with historical value.

The present study demonstrates that LIBS is a useful, promising and alternative technique for investigation of historical glasses, especially for those conserved under burial conditions and, generally speaking, for the study of non-destructible materials of cultural heritage. The speed of analysis achieved with this technique facilitates the examination of a large number of samples in the field, at an excavation site, or in a museum. Also, the development and production of portable LIBS devices alone or in combination with other analytical techniques,

which would enable analysis on site, are the subject of intense research, as technological advances offer more and more options for compact laser sources and detection equipment.

References

1   R. Noll, Laser-induced Breakdown Spectroscopy, Springer, 2012.

2   E. Tognoni, V. Palleschi, M. Corsi, G. Cristoforetti, Quantitative micro-analysis by laser-induced breakdown spectroscopy: a review of the experimental approaches, Spectrochim. Acta Part B 57 (2002) 1115-1130.

3   J.M. Vadillo, J.J. Laserna, Laser-induced plasma spectrometry: truly a surface analytical tool, Spectrochim. Acta Part B 59 (2004) 147–161.

4   D. W. Hahn, N. Omenetto, Laser induced breakdown spectroscopy (LIBS), part II: review of instrumental and methodological approaches to material analysis and applications to different fields, Appl. Spectrosc. 66 (2012) 347-419.

5   V. Lazic, F. Colao, R. Fantoni, V. Spizzicchino, Laser-induced breakdown spectroscopy in water: improvement of the detection threshold by signal processing, Spectrochim. Acta Part B 60 (2005) 1002-1013.

6   M. Hidalgo Nuñez, P. Cavalli, G. Petrucci, N. Omenetto, Analysis of sulfuric acid aerosols by laser-induced breakdown spectroscopy and laser-induced photofragmentation, Appl. Spectrosc. 54 (2000) 1805-1816.

7   Q. Sun, M. Tran, B.W. Smith, J.D. Winefordner, Determination of Mn and Si in iron ore by laser-induced plasma spectroscopy, Anal. Chim. Acta 413 (2000) 187-195.

8   I. Osticioli, J. Agresti, C. Fornacelli, I. T. Memmi, S. Siano, Potential role of LIPS elemental depth profiling in authentication studies of unglazed earthenware artifacts, J. Anal. At. Spectrom. 27 (2012) 827-833.

9   K.Melessanaki, M.Mateo, S.C. Ferrence, P.P. Betancourt, D. Anglos, The application of LIBS for the analysis of archaeological ceramic and metal artifacts, Appl. Surf. Sci. 197-198 (2002) 156-163.

10 A. Giakoumaki, K. Melessanaki, D. Anglos, Laser-induced breakdown spectroscopy (LIBS) in archaeological science-applications and prospects, Anal. Bioanal. Chem. 387 (2007) 749-760.

11 A. A. Bol'shakov, J. H. Yoo, C. Liu, J.R. Plumer, R.E. Russo, Laser-induced breakdown spectroscopy in industrial and security applications, Appl. Opt. 49 (2010) C132-C142.

12 B. Castle, K. Talabardon, B.W. Smith, J.D. Winefordner, Variables influencing the precision of laser-induced breakdown spectroscopy measurements, Appl. Spectrosc. 52 (1998) 649-657.

13 D. W. Hahn, N. Omenetto, Laser-induced breakdown spectroscopy (LIBS), part I: review of basic diagnostics and plasma-particle interactions: still-challenging issues within the analytical plasma community, Appl. Spectrosc. 64 (2010) 335- 366.

14 K.L. Eland, D.N. Stratis, D.M. Gold, S.R. Goode, S. Michael Angel, Energy dependence of emission intensity and temperature in a LIBS plasma using femtosecond excitation, Appl. Spectrosc. 55 (2001) 286-291.

15 A. Semerok, C. Chaléard, V. Detalle, J.L. Lacour, P. Mauchien, P. Meynadier, C. Nouvellon, B. Sallé, P. Palianov, M. Perdrix, G. Petite, Experimental investigations of laser ablation efficiency of pure metals with femto, pico and nanosecond pulses, Appl. Surf. Sci. 138-139 (1999) 311-314.

16 P. Stavropoulos, C. Palagas, G.N. Angelopoulos, D.N. Papamantellos, S. Couris, calibration measurements in laser-induced breakdown spectroscopy using nanosecond and picosecond lasers, Spectrochim. Acta Part B 59 (2004) 1885-1892.

17 A. De Giacomo, M. Dell'Aglio, A. Santagata, R. Teghil, Early stage emission spectroscopy study of metallic titanium plasma induced in air by femtosecond- and nanosecond-laser pulses, Spectrochim. Acta Part B 60 (2005) 935-947.

18 R.E. Russo, X.L. Mao, C. Liu, J. Gonzalez, Laser assisted plasma spectrochemistry: laser ablation, J. Anal. At. Spectrom. 19 (2004) 1084-1089.

19 J. Koch, A.A. Von Bohlen, R. Hergenröder, K. Niemax, Particle size distributions and compositions of aerosols produced by near-IR femto- and nanosecond laser ablation of brass, J. Anal. At. Spectrom. 19 (2004) 267-272.

20 V.Margetic, M. Bolshov, A. Stockhaus, K. Niemax, R. Hergenröder, Depth profiling of multi-layer samples using femtosecond laser ablation, J. Anal. At. Spectrom. 16 (2001) 616-621.

21 M. Corsi, G. Cristoforetti, M. Giuffrida, M. Hidalgo, S. Legnaioli, L. Masotti, V. Palleschi, A. Salvetti, E. Tognoni, C. Vallebona, A. Zanini, Archaeometric Analysis of Ancient Copper Artefacts by Laser-Induced Breakdown Spectroscopy Technique. Microchim. Acta 152 (2005) 1-2, 105-111.

22 A. Elhassan, A. Giakoumaki, D. Anglos, G.M. Ingo, L. Robbiola, M.A. Harith, Nanosecond and femtosecond Laser Induced Breakdown Spectroscopic analysis of bronze alloys. Spectrochim. Acta Part B 63 (2008) 4, 504-511.

23 V. Lazic, R. Fantoni, F. Colao, A. Santagata, A. Morone, V. Spizzichino, Quantitative laser induced breakdown spectroscopy analysis of ancient marbles and corrections for the variability of plasma parameters and of ablation rate. J. Anal. At. Spectrom. 19 (2004) 4, 429-436.

24 A. Erdem, A. Çilingiroğlu, A. Giakoumaki, M. Castanys, E. Kartsonaki, C. Fotakis, D. Anglos, Characterization of Iron age pottery from eastern Turkey by laser- induced breakdown spectroscopy (LIBS). J. Archaeol. Sci. 35 (2008) 9, 2486-2494.

25 P. Westlake, P. Siozos, A. Philippidis, C. Apostolaki, B. Derham, A. Terlixi, V. Perdikatsis, R. Jones, D. Anglos, Studying pigments on painted plaster in Minoan, Roman and Early Byzantine Crete. A multi-analytical technique approach. Anal. Bioanal. Chem. 402 (2012) 4, 1413-1432.

26 O. Kokkinaki, C. Mihesan, M. Velegrakis, D. Anglos, Comparative study of laser induced breakdown spectroscopy and mass spectrometry for the analysis of cultural heritage materials. J. Mol. Struct. 1044 (2013), 160-166.

27 K. Müller, H. Stege, Evaluation of the analytical potential of laser-induced breakdown spectrometry (LIBS) for the analysis of historical glasses. Archaeometry 45 (2003) 3, 421-433.

28 N. Carmona, M. Oujja, S. Gaspard, M. García-Heras, M.A. Villegas, M. Castillejo, Lead determination in glasses by laser-induced breakdown spectroscopy. Spectrochim. Acta B 62 (2007) 2, 94-100.

29 N. Carmona, M. Oujja, E. Rebollar, H. Römich, M. Castillejo, Analysis of corroded glasses by laser induced breakdown spectroscopy. Spectrochim. Acta B 60 (2005) 7-8, 1155-1162.

30 T. Palomar, M. Oujja, M. García-Heras, M.A. Villegas, M. Castillejo, Laser induced breakdown spectroscopy for analysis and characterization of degradation pathologies of Roman glasses. Spectrochim. Acta B 87 (2013), 114-120.

31 S. Klein, T. Stratoudaki, V. Zafiropulos, J. Hildenhagen, K. Dickmann, Th. Lehmkuhl, Laser-induced breakdown spectroscopy for on-line control of laser cleaning of sandstone and stained glass, Appl. Phys. A 69 (1999) 441.

32 C. Gerhard, J. Hermann, L.Mercadier, L. Loewenthal, E. Axente, C.R. Luculescu, T. Sarnetb, M. Sentis,W. Viöl, Quantitative analyses of glass via laser-induced breakdown spectroscopy in argon, Spectrochim. Acta B 101 (2014) 32-45.

33 E. Negre, V. Motto-Ros, F. Pelascini, S. Lauper, D. Denis, J. Yu, On the performance of laser-induced breakdown spectroscopy for quantitative analysis of minor and trace elements in glass, J. Anal. At. Spectrom. 30 (2015) 417-425.

34 J.D. Pedarnig, P. Kolmhofer, N. Huber, B. Praher, J. Heitz, R. Rössler. Element analysis of complex materials by calibration-free laser-induced breakdown spectroscopy. Appl. Phys. A 112 (2013) 105-111.

35 C. Isings, Roman Glass from Dated Finds. J.W. Wolter. Groningen, 1957.

36 R.W. Douglas, S. Frank, A History of Glassmaking, G.T. Foulis and Co. Ltd., London, 1972.

37 T. Palomar, M. García-Heras, R. Sabio, J.Ma. Rincón, M.A. Villegas, Composition, preservation and production technology of Augusta Emerita Roman glasses from the first to the sixth century AD, Medit. Archaeol. Archaeom. 12 (2012) 193-211.

38 D. Allen, Roman Glass in Britain, Shire Publications, Princes Risborough, Buckinghamshire, 1998.

39 C.M. Jackson, H.E.M. Cool, E.C.W. Wager, The manufacture of glass in Roman York, J. Glass Stud. 40 (1998) 55-61.

40 H.D. Smith, C.P. McKay, A.G. Duncan, R.C. Sims, A.J. Anderson, P.R. Grossl, An instrument design for non-contact detection of biomolecules and minerals on Mars using fluorescence, J. Biol. Eng. 8:16 (2014).

41 S.C. Hill, M.W. Mayo, R.K. Chang, Fluorescence of Bacteria, Pollens, and Naturally Occurring Airborne Particles: Excitation/Emission Spectra, Army Research Laboratory, Adelphi, MD 20783-1197, (www.dtic.mil/cgi-bin/GetTRDoc?AD=ADA494347) 2009.

42 E. V. Pestryakov, V. V. Petrov, V. I. Trunov, A. V. Kirpichnikov, A. G. Volkov, A. I. Alimpiev, A. Ja. Rodionov, $Be_3Al_2Si_6O_{18}$Crystals Doped with Jahn–Teller Ions:A Promising Active Media for Super broad band Lasers, Laser Phys. 11 (2001) 1138-1141.

43 R.W.B. Pearse, A.G. Gaydon, The identification of molecular spectra (third edition) Chapman and Hall Ltd, London 1963.

44 K.L. Eland, D.N. Stratis, T. Lai, M.A. Berg, S.R. Goode, S.M. Angel, Some comparisons of LIBS measurements using nanosecond and picosecond laser pulses, Appl. Spectrosc. 55 (2001) 279-285.

45 NIST electronic database, at http://physics.nist.gov/PhysRefData.

Table 1 Characteristics of studied Late Roman glasses.

Sample	Part number	Graveyard area	Thickness (mm)	Colour	Remarks
CS-1	21500-2 V1	1	1.1	Olive green	Dark deposits
CS-4	26100-3 V3	1	0.7	Colourless	Earthy deposits
CS-5	50500-2 V1	2	0.7	Colourless	Earthy deposits and bubbles
CS-7	50700-3 V1	2	0.6	Colourless	Earthy deposits and micro-cracks
CS-8	56400-1 V1	2	1.4	Yellowish colourless	Earthy deposits
CS-9	74300-2 V1	2	2.2	Bluish colourless	Iridescence layer and earthy deposits
CS-10	98400-1 V1	2	7.0	Blue	Dark deposits
CS-11	114100-1 V1	2	6.2	Olive green	Few earthy deposits
CS-12	114300-2 V1	2	0.7	Colourless	Earthy deposits

Table 2 Chemical composition in (wt..%) from XRF measurements carried out on historical glasses.

Sample	Na_2O	MgO	Al_2O_3	SiO_2	P_2O_5	SO_3	Cl^-	K_2O	CaO	TiO_2	MnO	Fe_2O_3	CuO	SrO	Sb_2O_3	BaO	PbO
CS-1	17.05	0.94	2.60	65.49	0.05	0.26	1.07	0.47	6.52	0.68	2.48	2.31	0.01	0.04	---	0.03	---
CS-4	16.05	0.68	2.49	67.01	0.13	0.36	0.94	0.75	9.89	0.08	1.07	0.50	0.01	0.04	---	---	---
CS-5	18.48	0.78	2.10	66.27	0.06	0.30	1.22	0.47	6.26	0.39	2.12	1.42	---	0.05	---	0.08	---
CS-7	18.96	1.08	1.92	63.71	0.07	0.33	1.24	0.36	8.60	0.21	2.01	1.42	---	0.07	---	0.02	---
CS-8	18.92	1.09	2.22	65.57	0.06	0.21	1.45	0.46	5.49	0.39	2.53	1.51	0.01	0.05	---	0.04	---
CS-9	18.70	0.54	1.93	67.83	0.12	0.31	1.33	0.71	7.15	0.10	0.36	0.64	0.01	0.04	0.18	---	0.05
CS-10	18.80	0.84	1.78	66.78	0.04	0.18	1.52	0.38	6.16	0.12	1.31	0.98	1.06	0.04	---	---	0.01
CS-11	17.71	0.91	2.22	67.85	0.05	0.24	1.28	0.40	5.00	0.44	2.27	1.52	---	0.04	---	0.07	---
CS-12	17.37	0.78	1.84	66.92	0.04	0.32	1.59	0.46	7.94	0.13	1.57	0.92	0.01	0.07	---	0.04	---

--- not detected

Table 3 Chemical composition in (wt.%) derived from XRF measurements carried out on standard an homemade model glasses.

Sample	Na$_2$O	MgO	Al$_2$O$_3$	SiO$_2$	P$_2$O$_5$	SO$_3$	K$_2$O	CaO	TiO$_2$	MnO	Fe$_2$O$_3$	Sb$_2$O$_3$	BaO	PbO	Cr$_2$O$_3$	B$_2$O$_3$	As$_2$O$_3$	ZrO$_2$
Gl-1	13.90	0.14	1.50	72.64	---	1.19	0.43	11.03	0.04	---	0.04	---	---	---	---	---	---	---
Gl-2	0.23	<0.02	0.05	56.34	---	---	11.85	<0.02	0.02	---	0.01	---	---	30.59	---	0.36	0.32	---
Gl-3	12.20	1.81	1.62	72.68	---	0.05	0.35	10.68	0.01	0.04	0.32	---	0.02	---	0.02	---	---	0.02
Gl-4	0.09	0.03	0.21	59.28	---	---	15.81	0.13	---	0.09	0.15	0.03	---	24.05	---	---	0.13	---
Gl-5	13.80	4.47	0.61	70.83	0.04	---	0.43	9.69	---	---	0.12	---	---	---	---	---	---	---
Gl-6	0.70	3.22	3.34	47.33	2.87	---	18.81	22.65	---	1.02	0.06	---	---	---	---	---	---	---
Gl-7	10.26	0.04	1.07	58.88	---	---	5.15	11.41	---	1.29	3.56	---	0.41	7.61	---	---	0.31	---

--- not detected

Table 4 Elements with their corresponding line emission wavelengths[45] used for determination of calibration curves with standard and model glass samples.

Element	Na I	Mg I	Al I	Si I	K I	Ca II	Ti I	Mn I	Fe I	Cu I	Ba II	Pb I	Cr I
Wavelength (nm)	330.23	285.21	309.27	288.16	404.41	317.93	453.32	403.07	438.35	324.75	455.40	405.78	520.84

Table 5 Elemental and chemical composition (wt.%) from LIBS measurements carried out on historical glasses using ns and fs laser pulses.

Sample	Na ns	Na fs	Mg ns	Mg fs	Al ns	Al fs	Si ns	Si fs	K ns	K fs	Ca ns	Ca fs	Ti ns	Ti fs	Mn ns	Mn fs	Fe ns	Fe fs	Cu ns	Cu fs	Ba ns	Ba fs	Pb ns	Pb fs	Cr ns	Cr fs
CS-1	20.90	21.30	2.35	2.70	3.50	1.35	61.95	61.70	0.80	1.65	1.90	3.80	1.20	1.10	2.45	1.30	3.80	3.00	---	---	0.10	0.10	0.45	0.04	0.15	0.08
CS-4	20.65	22.60	2.20	2.50	3.75	1.10	65.90	64.80	0.55	1.55	2.15	4.40	0.20	0.50	2.30	0.90	1.69	0.60	---	---	0.07	---	---	---	---	---
CS-5	21.16	22.65	0.90	1.90	1.55	1.20	64.10	64.70	0.25	1.10	6.60	3.65	0.40	0.20	1.20	1.15	2.70	1.15	---	---	0.25	0.20	0.15	0.60	0.05	---
CS-7	22.70	20.80	2.00	2.55	2.45	0.70	62.20	66.50	0.40	0.85	3.70	3.70	0.25	0.10	1.95	1.10	3.34	1.65	---	---	0.02	---	0.25	1.75	0.05	---
CS-8	21.30	22.20	1.50	2.45	2.20	1.00	63.30	65.10	0.45	0.95	3.30	3.80	0.70	0.15	2.45	0.90	4.08	1.50	---	---	0.09	0.05	0.30	0.83	0.07	0.04
CS-9	24.80	21.60	1.05	1.90	1.90	1.20	66.15	66.45	0.20	0.60	3.00	5.50	0.10	0.20	0.50	0.30	1.05	---	---	---	0.02	0.05	0.02	1.39	0.01	---
CS-10	22.95	21.00	1.40	2.25	1.80	0.50	64.55	63.90	0.20	1.70	4.60	4.80	0.05	0.45	1.00	0.60	1.27	0.60	1.05	1.05	0.02	---	0.12	1.68	0.03	---
CS-11	20.50	22.30	1.60	1.75	2.30	0.80	65.60	64.25	0.40	0.75	1.40	4.95	0.60	0.20	1.90	0.80	3.83	1.10	---	---	0.40	0.20	0.30	1.75	0.08	0.04
CS-12	24.25	23.85	1.10	1.75	1.60	0.70	64.60	65.15	0.20	0.75	4.15	4.10	0.10	0.20	1.25	0.35	1.49	0.20	---	---	0.08	0.04	0.10	1.70	0.02	---

-- not detected

Figure Captions

Fig. 1 Images of the selected Late Roman glass samples.

Fig. 2 UV-Vis spectra of glass samples: a) olive green CS-1, b) colourless CS-4, c) yellowish colourless CS-8, d) bluish colourless CS-9, e) blue CS-10. The labelled circles indicate the chromophores responsible of the observed bands.

Fig. 3 LIF spectra of representative Late Roman glasses upon excitation at 266 nm: a) olive green CS-1, b) colourless CS-4, c) yellowish colourless CS-8, d) bluish colourless CS-9, e) blue CS-10. Spectral resolution is 5 nm.

Fig. 4 Representative LIB spectra of historical glass sample CS-10 with: a) nanosecond and b) femtosecond laser excitation. The LIB spectra correspond to the accumulation of 15 laser pulses in the single pulse mode for ns pulses and to the accumulation of 50 laser pulses in the scanning mode for fs pulses. The time delay and gate width were 0 and 1 μs, respectively. The vertical units are comparable in the two figures.

Fig. 5 Calibration curves for: a) Na I, b) Mg I, c) Al I and d) Fe I for ns (panel on the left) and fs (panel on the right) laser pulses obtained by LIBS analysis of standard and model glass samples.
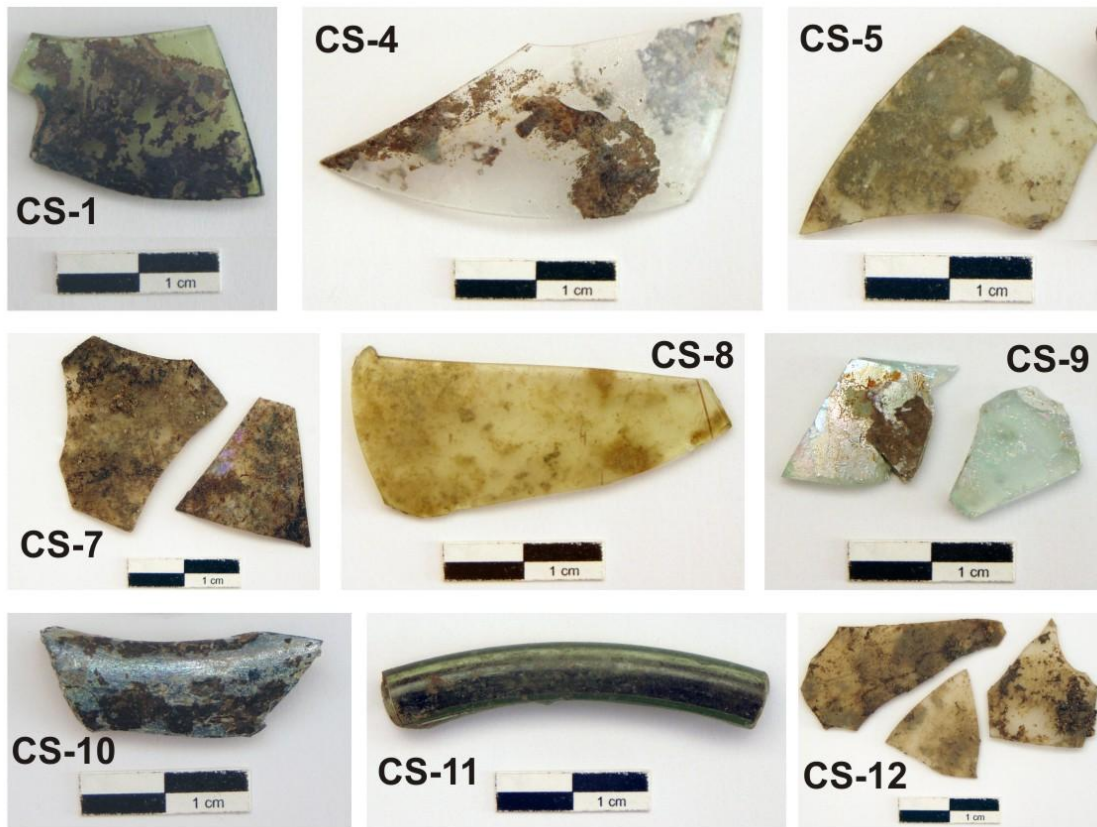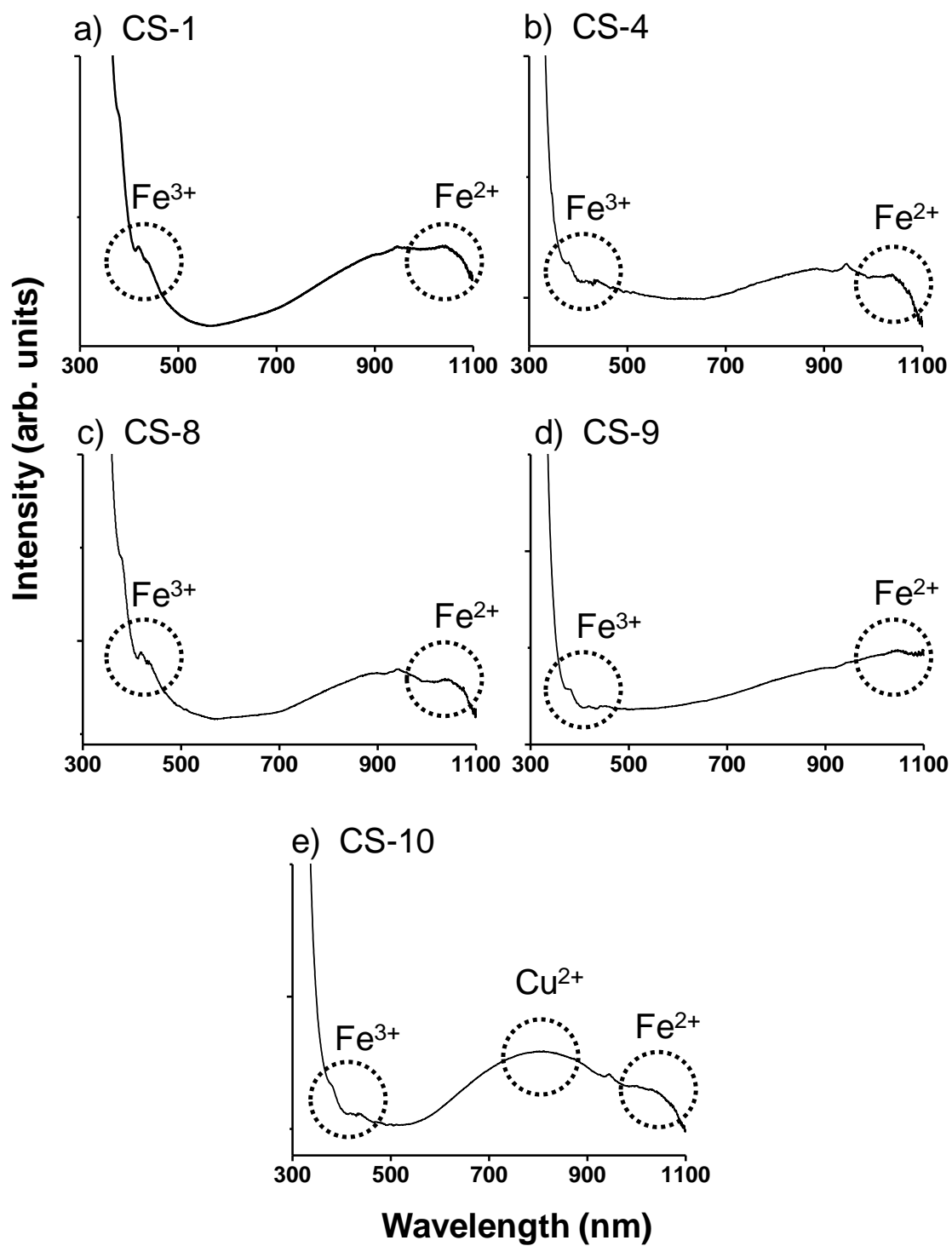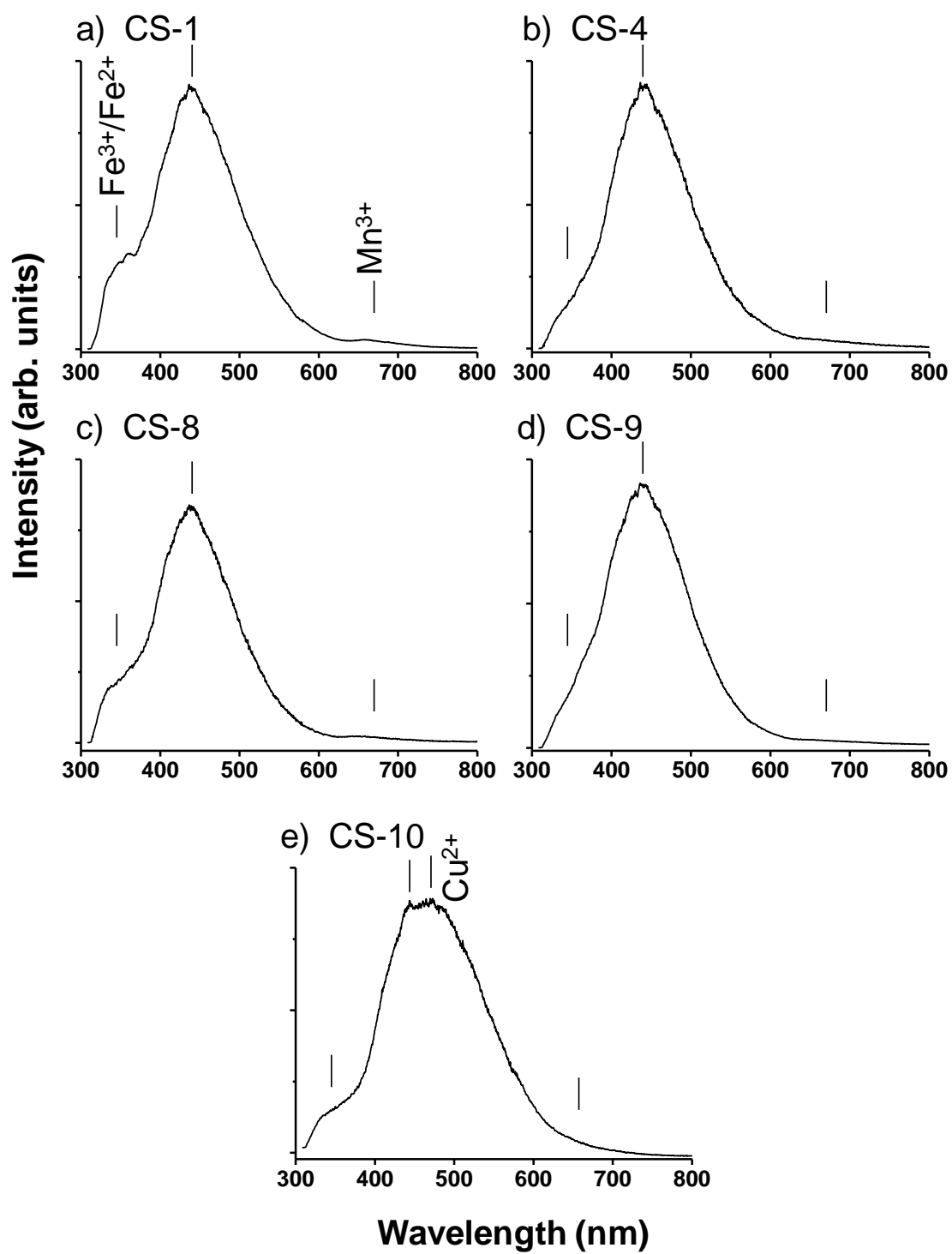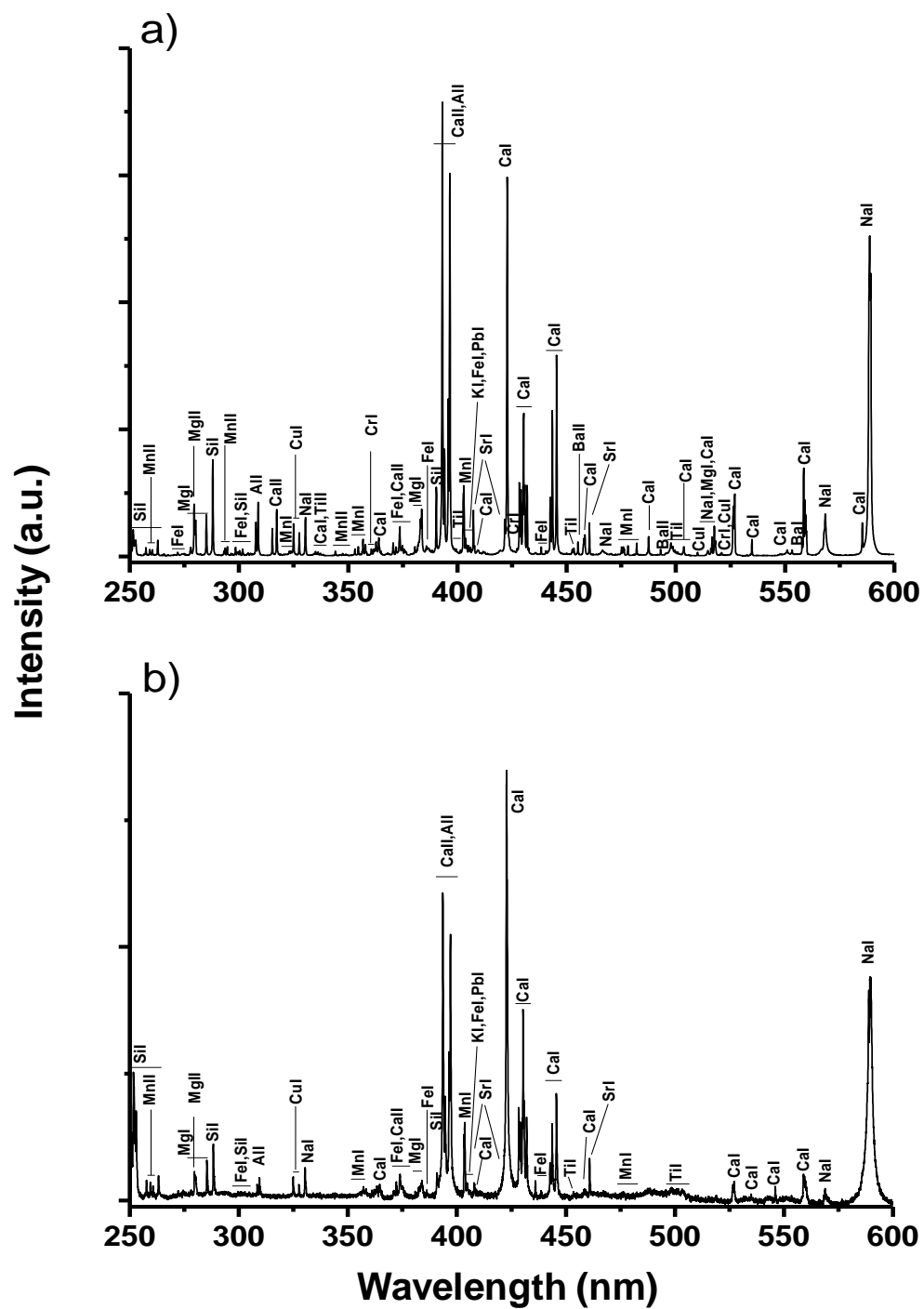
Fig. 1

Fig. 2

Fig. 2

a) CS-1

b) CS-4

c) CS-8

d) CS-9

e) CS-10

Fe^{3+} Fe^{2+} Cu^{2+}

Intensity (arb. units)

Wavelength (nm)

Fig. 3

Fig. 4

Fig. 5